COMBINING FULL SPHERICAL DEPTH AND HDR IMAGES TO IMPLEMENT A VIRTUAL CAMERA

Axel Waggershauser
SpheronVR AG, Germany
awagger@web.de

February 22, 2005

KEY WORDS: Image Based Lighting, Point Clouds, Registration, Rendering, Light Probe, HDR

ABSTRACT:

Based on a real-world scene description consisting of N spherical depth images from a laser range scanner and M spherical (high dynamic range) texture images we present a method that allows to place a virtual camera at an arbitrary position in the scene. The proposed method considers the position and orientation of each depth and texture scan respectively to be unknown. A possible application is to "capture" background images or light probes for photorealistic rendering. The first step to achieve this goal is to register the depth images relative to each other and mesh them, which is done by means of a combination of well known standard techniques. The next step is to register the texture scans relative to the geometry. For this purpose, we developed an error model, based on image coordinates of identified features in the depth and texture images, together with an appropriate minimization algorithm. The final step of "capturing" the new image is implemented with a ray-tracing based algorithm. The capabilities and remaining problems of this approach are discussed and demonstrated with high resolution real-world data.

1 INTRODUCTION

Creating photorealistic images or film sequences with both a real-world background and computer generated and animated objects is a very common task in most of todays film productions in the entertainment and advertising industry. This task needs the following entities of information: a) the background image, b) a full description of the artificial object, including geometric and reflectance (BRDF) properties, c) a complete description of the lighting situation at the position in 3-dimensional space where the artificial object should be inserted, i.e. what light (color and intensity) comes from which direction, and d) geometry information of, at least, the immediate surrounding area around the position where the artificial object should be inserted and according BRDF information for this geometry.

The necessity of the first two items is obvious, and they are readily available with state-of-the-art techniques. The third is necessary to correctly account for reflections and shadows on the artificial objects. It can be provided by a *light probe*, also called *radiance map*. This is sufficient if the new objects are far enough away from the real-world objects in the scene so that they do not noticeably affect their appearance, like dropping shadows to the floor, etc. But if the new objects do influence the old scene the fourth item is necessary as well [4]. As we will see, the background image might not be explicitly necessary, since it can be "captured" retrospectively with sufficient lighting and geometry information.

1.1 Light probe

A light probe for a 3D position x in the real-world environment W is a spherical image taken at position x that contains the color of incident light $L(x, \varphi, \vartheta)$ from W. I.e. every pixel of the light probe is associated with a direction (φ, ϑ) and its value describes the light coming from this direction. This information can be utilized by a renderer to illuminate the point x on a surface of an artificial object. This is referred to as *image based lighting*. To produce realistic results, *high dynamic range* (HDR) images are used. Compared to usual images with a dynamic range of 8 bits per color, they provide a wider range to store color values, especially the luminosity range is increased. There are a variety of different encodings and file formats with different accuracy and space requirement properties [15] available for storing HDR images.

Fig. 1: Full spherical HDR texture image (light probe) with its parameterization. The image has been tone mapped to reduce its dynamic range to enable an adequate output on paper.

The system used for capturing the HDR example images presented in this paper is the SpheroCam HDR, produced by SpheronVR AG. This camera system produces full spherical,

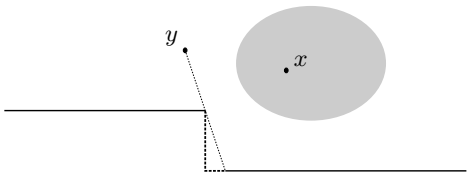

Fig. 2: A light probe taken in x cannot be used in y. Some parts of the light probe that are visible in point x should not be in y, for example the highlighted section of the wall.

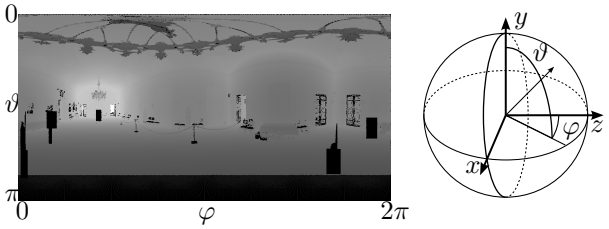

Fig. 3: Full spherical depth image with its parameterization and its associated local left hand coordinate system. The brighter the image pixel is, the further away is the respective object. The displayed range is approximately 1m to 25m.

high resolution HDR images in one shot. The image resolution is up to 50 mega pixels and the dynamic range goes up to 26 bits per color component. An example image is shown in fig. 1. Other means to produce HDR light probes and HDR images in general are presented in [4] and [5].

The objective of this work is to provide a method that allows to place a virtual camera at an arbitrary position in a real-world scene and "capture" background images or light probes for this position. This method is based on a real-world scene description consisting of N spherical depth images from a laser range scanner and M spherical (high dynamic range) texture images. Each image is captured at an unknown positions with unknown orientation.

1.2 Light probe restrictions

To correctly light the point x on a surface of an artificial object, one needs to have a light probe for exactly this position. In practice, however, a light probe for position x can be used to light positions in a region around x. The size and shape of this region depends on the geometry of the real-world scene. Fig. 2 illustrates the situation. The point y should not receive incident light from the highlighted section of the wall. This prohibits the usage of a light probe obtained at point x for lighting the point y. So relatively small objects might be lightable with a single light probe but the problem gets worse when an animation is to be rendered where the object moves across a real-world scene. In this case several light probes along the trajectory of the object are necessary.

This work reduces the number of necessary "real" light probes captured on site and allows to replace most of them with "virtual" light probes by utilizing geometry information. By projecting a light probe onto the scene's geometry, a raytracer can easily determine which parts of the light probe to consider when lighting a given point. In case the geometry and lighting information is sufficiently detailed and complete it is possible to extract background images as well.

A similar goal has been addressed already by [6] and [16]. Both proposals utilized photogrammetrically extracted geometry resulting in coarse approximations, which in turn produced obvious graphical artifacts in the resulting images. We have high resolution scans from the laser based depth measurement system Imager 5003, manufactured by Zoller+Fröhlich, available, which allow for an accurate and highly detailed geometry reconstruction of the scene.

1.3 Outline

The first step to achieve this goal is to register the depth images relative to each other and mesh them which is done by means of a combination of well known standard techniques, sketched in section 2. The next step is to register the texture scans relative to the geometry. For this purpose we developed an error model, based on image coordinates of identified features in the depth and texture images, together with an appropriate minimization algorithm which is presented in section 3. The final step of "capturing" the new image is implemented with a ray-tracing based algorithm, sketched in section 4. The capabilities and remaining problems of this approach are discussed and demonstrated with high resolution real-world data in the results section 5. Section 6 concludes this work and gives an outlook on possible future activities.

2 GEOMETRY RECONSTRUCTION

The goal of the geometry reconstruction performed by our approach is to be later on able to cast a ray from an arbitrary point inside the scene towards an arbitrary direction and be able to tell where that ray hits the surface of an object in the scene.

To accomplish this goal, the set of N "raw" spherical depth images has to be preprocessed. The value of each pixel in a depth image is a real number giving the distance between the scanner and the object that was hit by the laser. The coordinates of a pixel together with the depth value and the projection characteristics of the scanner define a 3D point in the *local* scanner coordinate system. This way each depth image is associated with a 3D point cloud (see fig. 3).

On the one hand, each of these point clouds is separately meshed into a set of triangles, representing patches of the surfaces of the objects in the scene. Each of those triangle meshes is then simplified to reduce the number of triangles. This is desirable to reduce the memory and computation time requirements of the subsequent rendering algorithm. On the other hand, a registration of the point clouds is performed to find the relative orientation and position of the individual scans. This results in a set of triangle meshes, registered relative to each other.

A comprehensive overview and comparison of the state of art techniques regarding geometry reconstruction can be found in several papers like [2, 3] and in the introductory part in [9].

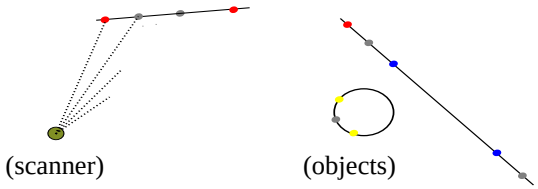

Fig. 4: Shown is a schematic 1D example scan including points of each class. Red dots belong to class *verge*, blue to *back edge*, yellow to *front edge*, and grey to *surface*.

2.1 Point classification

As a preparation, necessary for subsequent tasks like normal estimation, meshing, and registration, a classification of each pixel/point of the input images is performed. Based on itself and its neighbors, each point is assigned to one of the following classes:

- *invalid:* These are pixels with no useful distance information (e.g. the scanner does not receive enough light to estimate the distance). This classification is given by the scanner software.
- *verge:* These are the pixels next to an *invalid* pixel, i.e. pixels that have at least one neighbor with no distance information.
- *front/back edge:* These are the pixels at the near/far side of a local discontinuity, forming the edge/"shadow edge" of a contiguous surface patch.
- *surface:* These are the "good" points on an objects surface. They (should) constitute the biggest part of all points in the scans.

For an illustration of the different classes see fig. 4. This classification is not necessarily one-to-one, e.g. there may be pixels which are both *front edge* and *back edge* pixels at the same time.

The motivation behind the two edge classes is to be able to distinguish between points that have neighbors all belonging to the same surface patch and those that have neighbors belonging to different surface patches.

2.2 Registration

Given is a (fixed) *model* point cloud $\mathcal{M} \subset \mathbb{R}^3$ in the global or reference coordinate system $W_{\mathcal{M}}$ and a depth image with the associated (variable) *view* point set $\mathcal{V} \subset \mathbb{R}^3$ in the depth image's local coordinate system $W_{\mathcal{V}}$. Searched is the position and orientation of $\mathcal{V}$ in the reference coordinate system, i.e. a rigid transformation $T : \mathbb{R}^3 \to \mathbb{R}^3$ that maps the points in $\mathcal{V}$ from $W_{\mathcal{V}}$ to $W_{\mathcal{M}}$, so that $\mathcal{V}$ best matches $\mathcal{M}$. This function has 6 degrees of freedom, 3 translation and 3 rotation parameters. A straightforward way to represent T is a 3×3 rotation matrix R and a 3-element translation vector t with

$$T(p) = Rp + t. \tag{1}$$

When registering two views relative to each other, one of them can simply be defined as the model $\mathcal{M}$, so its local coordinate system becomes the global coordinate system. With more than two views, an obvious method is to pick a "central" view as $\mathcal{M}$ and process the remaining ones one after another.

The registration is further subdivided into a coarse and a subsequent fine registration. This is necessary since the used (fine) registration algorithms is basically a minimization algorithm for some error function and tends to get stuck in local minimum, hence, it needs a proper starting configuration provided as an initial value of R and t to find the global optimum. This is achieved by the coarse registration or pre-alignment step.

Coarse Registration The used method simply performs multiple (fine) registrations with different, evenly distributed start configurations and picks the one that fits best. The decision which fits best is based the error measure that the fine registration algorithm tries to minimize.

This approach is especially viable in case of spherical depth images with a high overlap because then both images contain virtually the same geometry information, and then the translation parameters t can be approximated by identifying the centers of mass of both point clouds. Furthermore, the remaining 3 degrees of freedom (the orientation) are usually de-facto reduced to 1 since the scanning device is usually always setup with its top pointing upwards. So, a small number, e.g. 8, of equally distributed horizontal "starting positions" for the scanner suffice to find the correct registration.

An interesting approach to establish a proper pre-alignment, which also works with non-full spherical scans, is based on so called *spin-images* and was presented in [11].

Fine Registration The fine registration algorithm used in our implementation is a variant of the widely known *iterative closest point* (ICP) algorithm. Many variants of the algorithm, originally introduced by [1], have been proposed. A comparison of available methods with a focus on efficiency can be found in [12].

The selection of corresponding point pairs in our ICP variant is based on a heuristic incorporating point distance, estimated normals and the point classification. For detailed information about the actual implementation see [14].

The update of the registration is performed by the closed-form solution for absolute orientation of a point set $\mathcal{V}$ with respect to $\mathcal{M}$ in presence of correspondence information $P \subset \mathcal{V} \times \mathcal{M}$ as given in [10]. Based on the point pairs in P, it calculates a rigid transformation T that minimizes the summed squared distance error

$$E(P) = \sum_{(v,m)\in P} \|T(v) - m\|^2. \tag{2}$$

This method separates the problem of finding T into first finding R then t. The first part is also used as a general purpose alignment method in an error metric used in the texture registration method in section 3.

2.3 Meshing

The meshing is quite straightforward, since the connectivity of the points is already given through their neighborhood relationship in the depth image. The pattern used for connecting the points is depicted in fig. 5. The only thing that has to be taken care of is to not connect points that belong to different surface

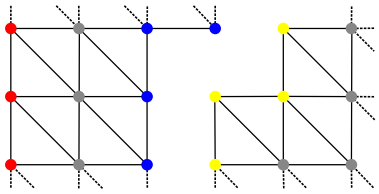

Fig. 5: Adjacent points in the depth image are connected to form a triangle mesh. Points from different surface patches are not connected. Red dots belong to class *verge*, blue to *back edge*, yellow to *front edge*, and grey to *surface*.

patches. This is achieved by assuring a triangle does not contain a *back edge* and a *front edge* point at the same time.

Simplification The number of triangles in the created meshes tend to become huge as the depth images may easily contain more than 10 million points, and for each point there are approximately two triangles in the generated mesh. For a typical scene, such a mesh is heavily oversampled, i.e. large patches of adjacent triangles lie on a plane and may be adequately described by only a view triangles. Therefore, a smaller set of triangles may be found, that still adequately describes the surfaces in the scene.

The simplification method used in this work was introduced in [8]. The reason, this approach was chosen, was mainly its availability as source code in the QSlim package [7]. We were able to reduce the number of triangles in our meshes by a factor of e.g. 100, which reduced the memory usage of the rendering application and increased its speed substantially.

3 TEXTURE REGISTRATION

The goal of registering the texture scans is basically the same as registering the geometry scans: find the position and orientation of the texture camera in the model coordinate system $W_{\mathcal{M}}$. The available input for solving this problem is the texture scan and the generated geometry model of the scene. The desired output is again a vector $t \in \mathbb{R}^3$ and a real 3×3 rotation matrix R, where t gives the position of the texture camera and R its orientation relative to the model coordinate system.

The algorithm used for solving this problem consists of two basic steps:

1. Selecting a number of so called *landmarks*, recognizable in texture and geometry, and establishing correspondences between each landmark's texture coordinates (2D) and its geometry coordinates (3D).
2. Finding position and orientation of the texture camera in the world coordinate system that does not contradict the correspondences found in step 1.

These two steps have to be performed for every texture image.

3.1 Establishing Texture – Geometry Correspondences

The texture-geometry correspondences are established by identifying features of the real-world scene that can be recognized in both representations, like edges, holes, etc. A clearly viable but also clearly cumbersome method is to manually establish these correspondences with interactive viewer applications allowing to pick and export coordinates. This is the way we gathered the data for our experiments.

Usually, laser range scanner systems do not only record the distance to a measured point, but also the intensity of the incident light, reflected by the surface of the measured object. Each pixel in the resulting grey scale image of the scene corresponds to one pixel in the associated depth image. This renders it possible in principal to automatically establish correspondences between features in the HDR texture images and the depth images by using the grey scale image as the bridging element. The correspondence between features in the color and the grey scale image may be established by means of image comparison, like the linear correlation coefficient.

Another way to utilize the accompanying grey scale image is to support the user in determining the landmark coordinates with sub-pixel accuracy and reduced noise. The additional information provides the crucial advantage that features, not recognizable in the depth image, namely the texture of the surface, may be recognizable in the grey scale image. This allows to select landmarks on flat patches of an object's surface. The distance of a landmark from the scanner may then be determined with the aid of a plane of best fit for the surrounding points. This may reduce the influence of noise of the single depth pixels considerably. Additionally, the angle coordinates of the landmark may be determined with sub-pixel accuracy by incorporating an appropriate comparison operator for the grey scale and color images.

3.2 Finding Position and Orientation

Some close research regarding the problem of finding position and orientation of a device by means of using position and bearing information of landmarks has been done in the context of autonomous mobile robot localization [13]. Most of these robots are some kind of wheel-driven vehicles, so their freedom of movement is usually restricted to two dimensions, namely the ground. Hence, the problem of localization is restricted to the plane, where only three degrees of freedom have to be determined: two for the position and one for the orientation. There are closed form solution available for this restricted problem. Our need for a solution in 3D lead to the development of a non-linear optimization algorithm for this purpose.

The following will describe the used error function, mapping the parameter space to the positive real numbers with a global minimum at the position in the parameter space that solves our problem and the algorithm that is capable of finding that minimum:

Error Function The input of step 2 is a list of N landmarks. Each landmark is given by its world coordinates $L^{\mathrm{G}} \in \mathbb{R}^3$ and its texture coordinates $L^{\mathrm{T}} \in \mathbb{T} = [0..w) \times [0..h)$ with w the width and h the height of the texture scan.

Each texture image is assigned a local coordinate system the same way as the depth images in section 2 (see fig. 1 and 3). This way, the texture coordinates are assigned a direction, which may be represented as a unit vector $v \in \mathbb{R}^3$ with $\|v\| = 1$. The (inverse) projection, mapping a texture coordinate to a unit vector, will be denoted by $P^{\mathrm{T}-1} : \mathbb{T} \to \mathbb{R}^3$.

An ordered set of unit vectors or the points on the unit sphere they correspond to, respectively, is called a *hedge hog* in the following. Ordered means, each is assigned a label or number, allowing to distinguish them. The i-th vector of a hedge hog H will be denoted by the subscript $H_{\langle i \rangle}$. The hedge hog model builds the fundamental base structure for the error function. The transformation of the texture coordinates of N landmarks into their unit vector representation results in such a hedge hog, which will be referred to as the *texture hedge hog*

$$H_T = \left\{ v = P^{\mathrm{T}^{-1}}(L_i^{\mathrm{T}}) \mid \forall\, 1 \leq i \leq N \right\}, \tag{3}$$

where $L_i^{\mathrm{T}} \in \mathbb{T}$ are the texture coordinates of the i-th landmark.

The error function is based on the idea that each position $p \in \mathbb{R}^3$ in the world coordinate system $W_{\mathcal{M}}$ may be assigned a (geometry) hedge hog

$$H_G(p) = \left\{ v = \frac{L_i^{\mathrm{G}} - p}{\|L_i^{\mathrm{G}} - p\|} \mid \forall\, 1 \leq i \leq N \right\}, \tag{4}$$

where $L_i^{\mathrm{G}} \in \mathbb{R}^3$ are the world coordinates of the i-th landmark. The elements of $H_G(p)$ give the directions of all N landmarks in the local coordinate system of p. This hedge hog $H_G(p)$ may then be compared with the texture hedge hog H_T to calculate the error $e(p)$ at p. Fig. 6 gives an example of the hedge hog definition for 2 dimensions.

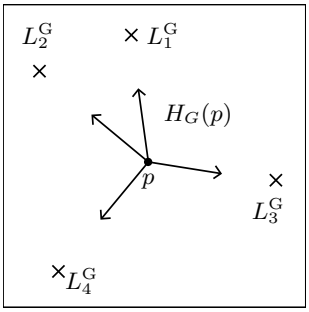

Fig. 6: A *hedge hog* $H_G(p)$ at position p is the ordered set of unit vectors pointing from p to L_i.

The goal of finding the position t and rotation R of the texture camera may be expressed with the introduced hedge hog model: find t and R such that $H_G(t) = RH_T$.

Motivated by the mentioned closed form solution for the problem in two dimensions, where position and orientation are found successively, we searched for an error function allowing the same separation in the 3D setup. This way, the parameter space for the non-linear minimization would be reduced from 6 to 3, resulting in a faster and more stable implementation. I.e. the error function has to be invariant with respect to the orientation of the hedge hogs. Different functions with this property have been evaluated. Best results have been obtained with the following error function:

$$e(p) = \sum_{i=1}^{N} \|H_G(p)_{\langle i \rangle} - AH_{T\langle i \rangle}\|^2 \tag{5}$$

where A denotes the rotation matrix, which minimizes the error $e(p)$. This is achieved by using the closed-form method already mentioned in section 2, introduced in [10]. Thus, $e(p)$ can be evaluated by first finding A and then actually calculate the sum of squared distances of equation (5).

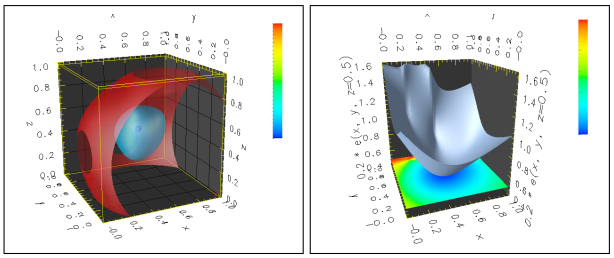

(a) (b)

Fig. 7: Example of an error function. The texture hedge hog $H_T = H_G((0.5, 0.5, 0.5)^T)$ is created at the center of the unit cube, which contains 5 randomly placed landmarks. (a) shows 3 iso-surfaces. (b) shows the slab at $z = 0.5$ plus the rubber sheet of that slab.

There is a faster and numerically more stable alternative which becomes evident after a closer look at the used algorithm to find A. In fact, the desired value $e(p)$ results as a byproduct from the calculation of A. Details are omitted here (see [14]). Fig. 7 shows an example of the error function.

After the optimal position t is found by minimizing $e(p)$ – which will be the subject of the next section – the optimal rotation matrix R, describing the orientation of H_T in $W_{\mathcal{M}}$, is given already. It is the error minimizing matrix A from equation (5).

Error Function Minimization The non-linear optimization algorithm, used to find the optimal estimate for t by minimizing the error function e: $t = \arg\min_p e(p)$, is an ad-hoc implementation of the idea of the steepest descent approach. The general structure of the algorithm is a loop which calculates successive estimates t_{k+1}, based on the last estimate t_k and the error function e, until a termination condition is reached. Given a current estimate t_k for t, the gradient Δe is numerically evaluated at t_k and used to indicate where the next estimate t_{k+1} should be placed. The steepest descent of e at t_k is in direction

$$d(t_k) = \frac{-\Delta e(t_k)}{\|\Delta e(t_k)\|}. \tag{6}$$

The next estimate t_{k+1} is then calculated by adding the vector $d(t_k)$, multiplied with a "step size" factor l, to t_k: $t_{k+1} = t_k + l \cdot d(t_k)$.

The idea behind l is similar to the adaptive step-size control in methods for solving differential equations, like the Runge-Kutta method. l is adjusted in each iteration of the algorithm. The adjustment is based on the difference between $d(t_k)$ and $d(t_{k+1})$. If the relative angle between $d(t_k)$ and $d(t_{k+1})$ is above a threshold, which is checked by evaluating the dot product $d(t_k) * d(t_k + l \cdot d(t_k)) < 0.8$, the current step size l was too big. It is then halved and a new $d(t_{k+1})$ is calculated. This is repeated until the threshold is exceeded. In case $d(t_k)$ and $d(t_{k+1})$ are sufficiently similar the step size may be increased to speed up the convergence.

The algorithm seems to be quite unselective regarding the start value t_0 in terms of finding the optimum value for t. Several experiments suggested that the error function has in general only one local minimum, which leads to a guaranteed convergence to the correct solution. This has not been proven, though. A suggesting start value is the centroid of the landmarks: $t_0 = \frac{1}{N} \sum_{i=1}^{N} L_i^{\mathrm{G}}$.

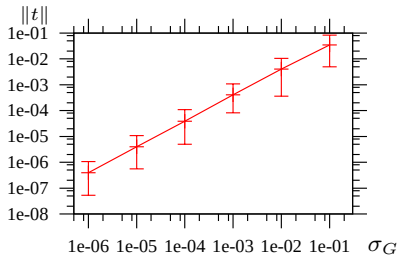

Fig. 8: Shown is the error $\|t\|$ of the final estimation for t depending on the noise in L_i^{G}. Displayed is the average, minimum, and maximum of 100 test-runs.

As the algorithm adjusts the step size l automatically during its execution, the initial value is not of great importance.

The algorithm is supposed to find a (local) minimum of e. At such a minimum, the gradient Δe vanishes. Thus, the algorithm terminates as soon as $\Delta e(t_k) < \tau$ falls below a small threshold.

Analysis of the Algorithm The described algorithm has been analyzed regarding its ability to find the correct solution for t depending on the following properties:

1. the level of noise in the landmark coordinates,
2. the number of landmarks N, and
3. the distribution of the landmarks.

The basic setup for all tests has been the same. Both algorithm inputs (the geometry and texture coordinates L_i^{G} and L_i^{T}) have been synthesized. N landmarks were randomly placed on the sphere with a radius of 10m. The input *texture hedge hog* has been simulated by synthesizing it from the geometry at the origin: $H_T = H_G(0)$. Hence, the "correct" solution for t was always the null-vector. This allowed for a simple measure for the quality of the result: $\|t\|$. Each test has been repeated a number of times and the average, the maximum, and the minimum value were used for interpretation. The obtained results and further details on the specific tests are presented in the following.

1. Level of noise in the landmark coordinates: The most dominant influence regarding the error in the algorithm output is noise. Both inputs, the geometry and the texture landmark coordinates, are subject to noise (scanning system and manual picking of coordinates). The noise has been simulated by adding a random variable vector with Gaussian distributed length and equally distributed direction after the creation of H_T to the geometry coordinates of the landmarks. Fig. 8a shows the error dependent on the standard deviation σ_G of the length of the noise vector. The number of landmarks used for this diagrams was $N = 10$. An expectable value for σ_G in real world data would be approximately 5mm. Randomizing H_T gives equivalent results.

2. Number of landmarks N: From the viewpoint of the user, the number of (necessary) landmarks should be kept as low as possible, since they are provided manually. The test showed, that the number should be at least 5. In the absence of noise, N is virtually insignificant. To double the precision one has to quadruple N, unfortunately. This effectively prevents the compensation of noise by increasing N.

3. Distribution of the landmarks: The most important aspect regarding the distribution of the landmarks is the coverage of the texture images with landmarks, i.e. the field of view that contains landmarks. The ability of the algorithm to come even close to the correct solution vanishes if the field of view is narrowed too much. A coverage of the sphere of less than about 15%, wich corresponds to a field of view of about $45°$, is insufficient. So the landmarks should be "spread all over" the sphere.

4 RENDERING

To capture an image with the virtual camera, each pixel is processed separately with a ray-tracing method, one after an other. To process one pixel one has to deeming the color of the light that incidents into position x from direction d, where x are the eye coordinates of the virtual camera given in the world coordinate system $W_{\mathcal{M}}$.

First of all, a short summary of the preprocessings' results: The geometry reconstruction step yielded N triangle sets G_i with associated rigid transformations $T_i^{\mathrm{G}}(p) = R_i^{\mathrm{G}}(p) + t_i^{\mathrm{G}}$, aligning those sets with the reference coordinate system $W_{\mathcal{M}}$. The texture registration step yielded M rotation matrices R_j^{T} and positional vectors t_j^{T}, describing the orientation and position of the associated M texture images T_j in $W_{\mathcal{M}}$.

To determine the color of the light engaging in x from direction d, the ray $x + rd$, with $r \in \mathbb{R}_+ \cup \{\infty\}$, is intersected with all N triangle sets $T_i^{\mathrm{G}}(G_i)$.

This yields N intersections r_i. The case where $x + rd$ does not intersect any triangle in $T_i^{\mathrm{G}}(G_i)$ is represented by $r_i = \infty$. Those N r_i are very likely different. Due to incomplete geometries some of them might be infinite and the others are suspect to registration errors and noise. From this contradicting set of intersections a single value

$$\bar{r} = \sum_{i=1}^{N} \mu_i r_i \tag{7}$$

is distilled by weighting the individual r_i. Our current implementation simply picks the closes intersection: $\bar{r} = \arg\min_i r_i$. Other weightings, incorporating more of the r_i, might be used to smooth the surfaces.

With $\bar{r}$, the position of the light source $p_d = x + \bar{r}d$ of direction d has been found. The next step is to determine its color c_d. Therefore, p_d is transformed into the local coordinate system of each of the M texture images with the inverse $R_j^{\mathrm{T}^{-1}}$ and t_j^{T} and then projected into texture coordinates with the appropriate projection function $P_j^{\mathrm{T}} : \mathbb{R}^3 \to \mathbb{T}$ for the respective texture camera:

$$p_d \to (x_j, y_j) = P_j^{\mathrm{T}}(R_j^{\mathrm{T}^{-1}}(p_d - t_j^{\mathrm{T}})) \in \mathbb{T} \,. \tag{8}$$

Finally, c_d is calculated by summing the weighted colors from each texture image T_j at the respective coordinates:

$$c_d = \sum_{j=1}^{M} \nu_j T_j(x_j, y_j) \,. \tag{9}$$

The most obvious constraint for the weights ν_j is that only those images T_j with an unobstructed line of sight from their position

t_j^{T} to p_d may contribute to c_d (see fig. 9). If any object was between t_j^{T} and p_d, the pixel $T_j(x_j, y_j)$ has seen this object, not the surface at p_d. On account of this, for each texture T_j, the ray $t_j^{\mathrm{T}} + r \cdot (p_d - t_j^{\mathrm{T}})$ is tested for intersection with the complete triangle set $G = \bigcup\ T_i^{\mathrm{G}}(G_i)$. If there was an obstacle, the weight ν_j is set to 0. The other texture images might contribute to c_d.

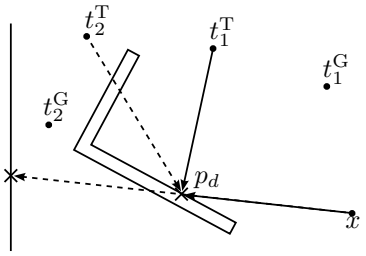

Fig. 9: Occlusions in texture images have to be considered in the weighting process. The texture at t_2^{T} may not contribute to the color of point p_d, since it is occluded.

Different weightings have been tested. Using only the texture closest to p_d leads to the highest local resolution but produces visible artifacts at the transition boundary (fig. 11f). Averaging all valid textures blurs the result due to registration errors. Best results have been obtained by weighting the textures proportional to their reciprocal distance to p_d raised to a power.

There are exceptional cases, which need special handling. If all r_i from equation (7) are equal to ∞ there is no intersection of the ray $x + rd$ with any triangle in the set G. For indoor scenes, which we focused on, this usually means there was no depth scan covering the respective geometry. In this case we simply set the color c_d to black (fig. 11a). A similar problem arises when a proper position p_d has been found but no texture information for this point is available.

5 RESULTS

The presented example renderings in this work are based on depth and HDR texture images captured in the *Kaisersaal* in the historic city hall of *Hamburg*, Germany (fig. 10).

The images of fig. 11 show some example renderings, generated with the proposed techniques. They reveal some serious quality deficiencies:

Black holes: Missing geometry or texture information results in black holes (fig. 11a). A simple workaround is to interpolate those black pixels in the image with the surrounding non-black pixels, as shown in fig. 11b. For lighting purposes this might be satisfying, but in background images this is no satisfying solution for large patches of missing information like the doorway. The only real solution for this is to add more texture and geometry scans, containing the missing information.

Overlooked geometry: If certain real-world objects are to small to be sufficiently sampled by the laser scanner to form representing triangle representations, they are missing in the geometry model. An example is the red barrier rope in fig. 11c. Sudden depth changes near object edges pose problems to the laser scanner, too (fig. 11f). This leads to falsely positioned texture information. For lighting purposes, this is usually no problem, except

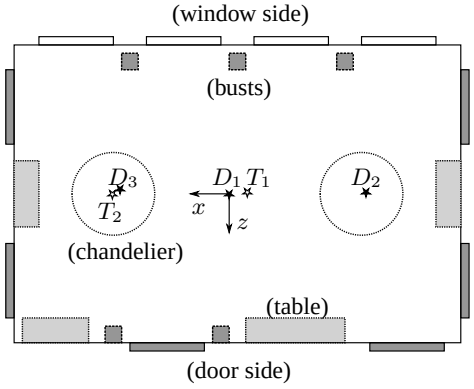

Fig. 10: Floor plan of the *Kaisersaal*, including the positions of the texture images $T_{1,2}$ and the depth images $D_{1,2,3}$. The local coordinate system of D_1 is the model coordinate system. The texture image of fig. 1 is T_1 and the depth image in fig. 3 is D_2.

the texture of those small objects is crucial for lighting, which is the case for the light bulbs of the chandelier in fig. 11c. For background shots, even the rope on the ground might be considered distracting.

Insufficient texture registration precision: Other than the first two items, which are rather a problem of inadequate input than a problem of the proposed methods, this one applies to the latter. The puniest error in the registration of the texture causes visibly falsely positioned color information near edges of real-world objects (fig. 11e) and at seams where different textures are blended (fig. 11f).

The answer to the question of where the virtual camera can be placed relative to the captured real-world geometry depends on the demand for the resulting quality. The closer one comes to patches of missing or wrongly registered geometry and texture features, the worse become the rendering results. For (nearly) closed topologies, like an indoor room, it is obvious that only positions *inside* the room are valid.

6 CONCLUSION

A method for combining depth and HDR texture images to implement a virtual camera has been presented. This allows to render photorealistic sequences with moving objects inside real-world scenes.

Remaining problems of the proposed method are in particular the manual establishing of texture and geometry feature correspondences in the texture registration step. This is cumbersome and error prone.

The presented approach has several open ends and space for further research:

- improved texture-depth feature correspondence establishing by incorporating sub-pixel accuracy and averaging techniques to reduce noise
- support for non-full-spherical scans as input and
- better heuristics to deal with missing geometry and texture information.

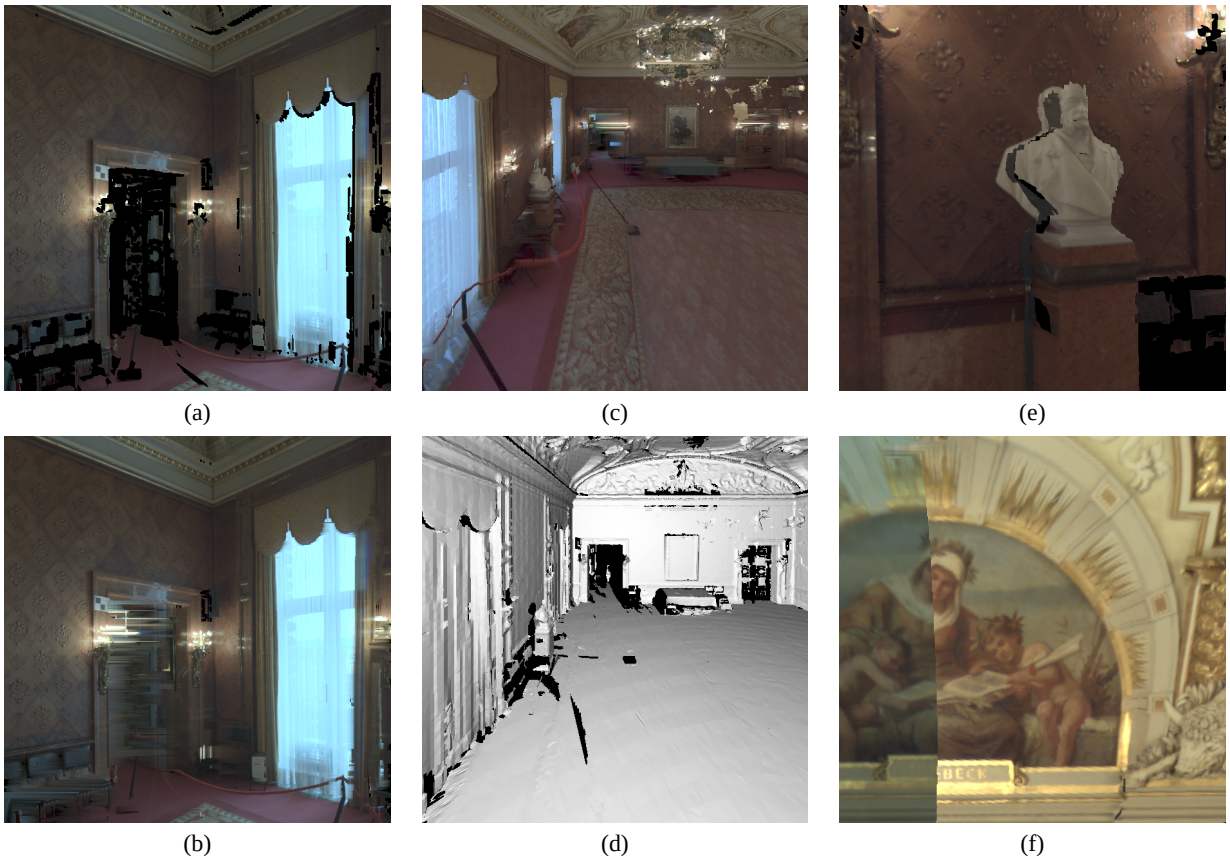

Fig. 11: The most obvious quality problems in the background shots are: missing geometry and texture information (a, b); overlooked geometry (c, d); and insufficient texture registration precision (e, f).

Acknowledgements Thanks to the courtesy of Zoller+Fröhlich, SpheronVR, and Professor Kersten – Hochschule für Angewandte Wissenschaften Hamburg for the sensor data this work has been based on and to Thomas Kollig for his support during the creation of my thesis, which this paper was based on.

References

[1] P. Besl and N. McKay. A method for registration of 3-d shapes. *IEEE Transactions on Pattern Analysis and Machine Intelligence*, 14(2):239–256, February 1992. 2.2

[2] R. J. Campbell and P. J. Flynn. A survey of free-form object representation and recognition techniques. *Comput. Vis. Image Underst.*, 81(2):166–210, 2001. 2

[3] G. Dalley and P. Flynn. Pair-wise range image registration: a study in outlier classification. *Comput. Vis. Image Underst.*, 87(1-3):104–115, 2002. 2

[4] P. Debevec. Rendering synthetic objects into real scenes: Bridging traditional and image-based graphics with global illumination and high dynamic range photography. *Computer Graphics*, 32(Siggraph '98 Proceedings):189–198, 1998. 1, 1.1

[5] P. Debevec and J. Malik. Recovering high dynamic range radiance maps from photographs. *Computer Graphics*, 31(Siggraph '97 Proceedings):369–378, 1997. 1.1

[6] P. Debevec, Y. Yu, and G. Boshokov. Efficient view-dependent image-based rendering with projective texture-mapping. Technical Report CSD-98-1003, 20, 1998. 1.2

[7] M. Garland. qslim 2.0. URL `http://graphics.cs.uiuc.edu/~garland/software/qslim20.html`. 2.3

[8] M. Garland and P. S. Heckbert. Surface simplification using quadric error metrics. *Computer Graphics*, 31(Annual Conference Series):209–216, 1997. 2.3

[9] A. Grün and D. Akca. Least squares 3d surface matching. In *The ISPRS International Archives of the Photogrammetry, Remote Sensing and Spatial Information Sciences*, volume XXXIV 5/W16, 2004. 2

[10] B. K. P. Horn. Closed form solution of absolute orientation using unit quaternions. *Journal of the Optical Society of America A*, 4(4):629–642, April 1987. 2.2, 3.2

[11] A. Johnson and M. Hebert. Surface registration by matching oriented points. In *Proc. Int. Conf. on Recent Advances in 3-D Digital Imaging and Modeling*, pages 121–128, 1997. 2.2

[12] S. Rusinkiewicz and M. Levoy. Efficient variants of the ICP algorithm. In *Proceedings of the Third Intl. Conf. on 3D Digital Imaging and Modeling*, pages 145–152, 2001. 2.2

[13] I. Shimshoni. On mobile robot localization from landmark bearings. *IEEE Transactions on Robotic and Automation*, 18(6):971–976, 2002. 3.2

[14] A. Waggershauser. Photorealistic rendering from depth and hdr images. Diploma thesis. Technische Universität Kaiserslautern, 2004. 2.2, 3.2

[15] G. Ward. High dynamic range image encodings. URL `http://www.anyhere.com/gward/hdrenc/hdr_encodings.html`. 1.1

[16] M. Wicke. Photorealistic rendering from high dynamic range panorama scans. Diploma thesis. Universität Kaiserslautern, 2003. 1.2